Design and Quasistatic Modelling of Hybrid Continuum Multi-Arm Robots

Zisos Mitros[1], S.M.Hadi Sadati[1], Sotirios Nousias[1], Lyndon Da Cruz[2,*] and Christos Bergeles[1,*]

***Abstract*— Continuum surgical robots can navigate anatomical pathways to reach pathological locations deep inside the human body. Their flexibility, however, generally comes with reduced dexterity at their tip and limited workspace. Building on recent work on eccentric tube robots, this paper proposes a new continuum robot architecture and theoretical framework that combines the flexibility of push/pull actuated snake robots and the dexterity offered by concentric tube robotic end-effectors. We designed and present a prototype system as a proof-of-concept, and developed a tailored quasistatic mechanics-based model that describes the shape and end-effector's pose for this new type robotic architecture. The model can accommodate an arbitrary number of arms placed eccentrically with respect to the backbone's neutral axis. Our experiments show that the error between model and experiment is on average 3.56% of the manipulator's overall length. This is in agreement with state of the art models of single type continuum architecture.**

I. Introduction

Continuum robots are actuatable structures that can conform to continuous curves. Therefore, surgical continuum robots promise to make interventions less invasive and more accessible as they can follow complex curved paths through body lumen and tissue deep inside the human cavity while minimising collateral damage [1]. Such flexible robots have been proposed for several interventions such as cardiac surgery [2], eye surgery [3]–[5], distal lung sampling [6], [7] and transurethral surgery [4], [8].

Continuum robots can be categorized based on their structural design and actuation architecture. For the purposes of this paper, notable continuum robots are the multibackbone continuum robots [1] and concentric tube robots (CTRs) [9]. Multibackbone systems were introduced in [10], and are typically composed of multiple elastic elements, rods or tubes, that run in parallel [11]. Their shape is usually constrained by fixtures that have holes for the rods or tubes to pass. A central backbone exists to which those fixtures are rigidly connected, while the elastic elements are attached to the last fixture of a bending section [12]. These systems offer high manipulability with a large reachable workspace however, they can lead to large path deviation errors when paths with two or more different curvatures need to be traversed [13].

This research was supported by an ERC Starting Grant [714562], the Wellcome Trust/EPSRC [203145Z/16/Z], and core funding from the Wellcome/EPSRC Centre for Medical Engineering, Wellcome Trust [WT203148/Z/16/Z].

[1]Z. Mitros, S.M.H. Sadati, S. Nousias, and C. Bergeles are with the Robotics and Vision in Medicine (RViM) Lab, School of Biomedical Engineering & Imaging Sciences, King's College London, London, UK. Z. Mitros is also with the Department of Medical Physics and Biomedical Engineering, University College London, London, UK. [2]L. Da Cruz is also with Moorfields Eye Hospital, London, UK. Correspondence: zisos.mitros.17@ucl.ac.uk * denotes equal contribution.

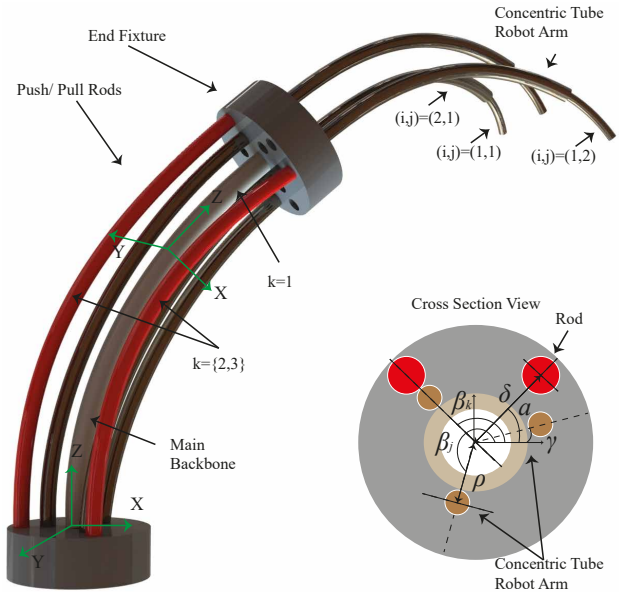

Fig. 1. Schematic of the continuum robot with one bent segment and three eccentrically arranged concentric tube robot (CTR) arms. Each arm comprises two nitinol tubes. The central backbone of the push/pull segment is modelled as a Cosserat rod. The cross section unit depicts the position of the push/pull rods and the CTR arms with respect to the central backbone.

Concentric Tube Robots (CTRs) are also extrinsically actuated. They comprise precurved elastic tubes that conform to a mutual shape [14], [15]. The independent translation and rotation of each tube results in the control of the shape of the robot and tip pose. CTRs are mainly made of nitinol (NiTi) because of its super-elastic and shape memory properties. As the tubes' diameter decreases, the elastic range of robot curvature increases and with it robot dexterity. Therefore, CTRs can catalyse novel medical applications that require tip dexterity, as thoroughly reviewed in [9]. However, the range of shapes that a CTR can achieve is limited and determined by the tubes' design (precurvature and curved length). This is a limiting factor as CTRs end up needing an application-based design optimization, explicit path-planning techniques, and commonly possess non convex workspaces [16].

Hybrid systems can combine the advantages of both categories and overcome their constraints. The tip dexterity of CTRs can be retained while their workspace can expand and made convex through the use of a push/pull actuation system as a driving backbone. Building on our and recent work on eccentric tube robots [11], [17]–[19], we designed, prototyped, modelled, and experimentally evaluated a multi-arm hybrid continuum robot. Its navigation section, responsible for anatomy navigation and coarse positioning of the

robot tip, is a push/pull actuated section comprising NiTi rods and a backbone on which fixtures with holes are rigidly connected. In contrast to a cable driven system, the proposed design offers more bending curvature as the rods, because of their greater diameters, can be also pushed. Its manipulation section, responsible for performing the surgical task, comprises of CTR arms, passing through the fixtures' holes. The proposed architecture combines the flexibility and capability for conformance to the anatomy of multibackbone robots be combined with the tip dexterity offered by CTRs.

It is envisioned that this kind robot can be used, for example, in deep orbital interventions and more specifically in Optic Nerve Sheath Fenestration [3]. In [3], we proposed to employ CTRs through a bespoke rigid collimator that is sutured on the eye sclera to access the optic nerve and perform the required task. A flexible navigation section, as the proposed push/pull section, can substitute the collimator and enhance the workspace and the dexterity of the system. In [6], we showed that push/pull systems can traverse tightly curved 3D paths in confined spaces. This work is the first step towards the development of hybrid systems able to navigate inside the human body and deliver dexterous manipulation arms close to the surgical area of interest.

The rest of the article is organized as follows. Section II develops a mechanics-based quasistatic kinematic model for the proposed hybrid continuum robot, considering an arbitrary number of push/pull actuated bending segments and CTR arms. Section III presents the architecture of the continuum robot prototype comprising of one push/pull actuated segment and 3 CTR arms. Experimental evaluation of the proposed model in loaded and unloaded cases is described in Section IV. Section V concludes the article.

II. Modeling and Theoretical Analysis

This section presents a mechanics-based kinematic model for the proposed hybrid continuum robot architecture, based on the Cosserat-rod theory [20]. The proposed model can be used in small scale movements, as those in robotic surgeries, in contrast to the model of [21] which is a geometric one and its accuracy is low mainly due to the effect of constant curvature. To derive the model, we employ the assumptions of the classical elastic-rod theory of Kirchhoff [14]:

- The backbone, the rods and the tubes are axially rigid and no cross-sectional shear deformation is presented.
- Deformation of the tubular components is entirely due to bending.
- The fixtures are rigid. They are perpendicular to the central backbone while their holes are big enough for the CTR arms to pass.
- The weight of fixtures, central backbone, rods and CTR arms is negligible and not taken into account.

The following notation is used throughout the paper: x, $\mathbf{x}$, and $\mathbf{X}$ denote a scalar, a vector, and a matrix, respectively. The prime denotes derivation with respect to the spatial coordinate s. Subscript $j = 1, \cdots, N$ denotes the CTR arm of the robot referred to within the equations, while subscript $i = 1, \cdots, N$ the ith tubular component. The tubular components of the push/pull section is denoted by $k = 1, \ldots, N$, with $k = 1$ referring to the backbone of the navigation section. A schematic of the proposed hybrid multi-arm continuum robot architecture is shown in Fig. 1. The relative position of each rod of the navigation section and each CTR arm with respect to the backbone is:

$$\begin{aligned} \boldsymbol{d}_k &= [\delta_k \cos(\beta_k), \quad \delta_k \sin(\beta_k), \quad 0]^T, \\ \boldsymbol{p}_j &= [\rho_j \cos(\beta_j), \quad \rho_j \sin(\beta_j), \quad 0]^T, \end{aligned} \tag{1}$$

where δ_k, ρ_j are the distances of the rods, and CTR arms, from the robot's central backbone, respectively. Variables β_k, β_j are the angles of the k^{th} push/pull rod, and j^{th} CTR arm, with respect to the central backbone. While not necessary, angularly distributing the rods and CTR arms is a sensible design choice:

$$\begin{aligned} \beta_k &= \gamma + (k-2)\gamma_{rod}, \quad k \neq 1, \\ \beta_j &= \alpha + (j-1)\frac{2\pi}{n}, \end{aligned} \tag{2}$$

with α and γ shown in Fig. 1 and n the number of CTR arms and γ_{rod} the angle between two subsequent rods. Please note that a certain number of fixtures is employed to avoid buckling of the push/pull rods.

The robot's central backbone is modelled as a long, slender, one-dimensional Cosserat rod endowed with a continuous homogeneous transformation matrix attached to every point on its arc. Figure 2 shows the modelling of each tubular component as a Cosserat rod under an arbitrary distributed force and/or point force. A unique set of 3D centroids, $\boldsymbol{r}(s) : [0, \ell] \times [0, \infty] \rightarrow \mathbb{R}^3 \times [0, \infty]$, and a family of orthogonal transformations, $\mathbf{R}(s) : [0, \ell] \times [0, \infty] \rightarrow so(3) \times [0, \infty]$ is employed to compute the position and orientation of the central backbone which is defined as:

$$\boldsymbol{r}^{'}(s) = \mathbf{R}(s)\boldsymbol{e}_3, \quad \mathbf{R}^{'}(s) = \mathbf{R}(s)[\mathbf{u}(s)]_{\times}, \tag{3}$$

where $\boldsymbol{u}(s) = [u_x(s), u_y(s), u_z(s)]^T$ is the curvature vector of the deformed backbone and comprises the kinematic variables of the modelling problem. The unit vector, $\boldsymbol{e}_3 = [0,\ 0,\ 1]^T$, is aligned with the z-axis of the global coordinate frame while $[.]_{\times}$ operator is the isomorphism between a vector in $\mathbb{R}^3$ and its skew-symmetric cross product matrix.

Transition points divide the robot's length into segments. The transition points are where a tube goes from straight to curved, where a tube ends, and where the push/pull section ends and the CTR arms begin. Segments and sections are later connected to each other by enforcing the continuity of shape and internal moment.

To derive the curvature of the central backbone in the navigation section, the derivatives of the force and moment balance with respect to the arc length s are calculated as in [14]. Please note that we dropped s for simplicity:

$$\begin{aligned} \sum_{k,i,j=1}^{n} (\mathbf{n}^{'}_{k,i,j} + \mathbf{f}_{k,i,j}) = 0, \\ \sum_{k,i,j=1}^{n} (\mathbf{m}^{'}_{k,i,j} + \mathbf{e}_3 \times \mathbf{n}_{k,i,j} + \mathbf{l}_{k,i,j}) = 0. \end{aligned} \tag{4}$$

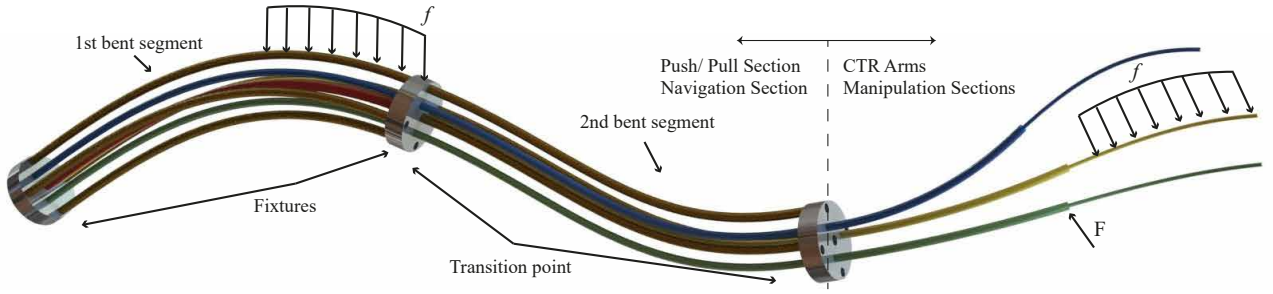

Fig. 2. Schematic of a multi-backbone robot with two bending segments and three CTR arms, all under an arbitrary external distributed force.

where $\mathbf{m}, \mathbf{n}$ are the internal moment and force respectively while $\mathbf{f}, \mathbf{l}$ are distributed force and moment respectively along its length. A linear constitutive law is employed to relate the kinematic variable $\mathbf{u}$, to the derivative of the internal moment, $\mathbf{m}'$:

$$\mathbf{m} = \mathbf{K}(\mathbf{u} - \mathbf{u}^*), \tag{5}$$

where $\mathbf{u}^*$ is the precurvature of the i^{th} tube of the j^{th} arm.

The curvature of each tubular component is related to curvature of the central backbone as:

$$\mathbf{u}_i = (\mathbf{R}^T_{\theta_{k,i,j}} \mathbf{u}_{k=1} + \theta'_{k,i,j}\mathbf{e}_3)/(1 + \mathbf{e}_3^T[\mathbf{u_{k=1}}]_\times \mathbf{R}_{\theta_i} \boldsymbol{d}_{ec}) \tag{6}$$

where $\mathbf{d}_{ec} \equiv \mathbf{d}_k$ for the rods and $\mathbf{d}_{ec} \equiv \mathbf{p}_j$ for the arms while $\mathbf{R}_{\theta_k} \equiv \mathbf{I}$ for the rods comprising the navigation section.

Following the methodology in [14] and employing (4), (5) and (6), the differential equation of the backbone's curvature becomes:

$$\begin{aligned} \boldsymbol{u}'_{k=1} = -\mathbf{K}^{-1}\Bigg[& \sum_{k=1}^{n} [\mathbf{u}]_\times \mathbf{K}_k \boldsymbol{u_{k=1}} + \sum_{j=1}^{n}\sum_{i=1}^{n} \mathbf{K}_{i,j}\theta'_{i,j} \\ & \frac{\mathrm{d}\mathbf{R}^T_{\theta_{i,j}}}{\mathrm{d}\theta_{i,j}} \boldsymbol{u_{k=1}} + [\mathbf{u}]_{\times_{i,j}} \mathbf{K}_{i,j}(\mathbf{u}_{i,j} - \mathbf{u}^*_{i,j}) \\ & + [\boldsymbol{e}_3]_\times \mathbf{R}^T(l-s)f + {\mathbf{R}_1}^T\mathbf{l}\Bigg]. \end{aligned} \tag{7}$$

In (7), $\mathbf{K}_{i,j}$ and $\mathbf{K}_k$ are the stiffness matrices of each CTR tube and push/pull rod respectively, while $\mathbf{K} = \mathrm{diag}(EI, EI, GJ)$ is the stiffness matrix for the whole robot; E is the robot's Young's modulus; I is the second moment of inertia; G is the shear modulus; J is the polar moment of inertia and l is the length of the central backbone.

Please note that the rods of the navigation section are rigidly connected to the last fixture of the segment that they actuate. As a result, they do not experience torsion. On the other hand, the tubes that comprise the CTR arms can freely pass from the fixtures' holes. We employ an angle, $\theta_{i,j}$ to model the relative rotation of the i^{th} tube of the j^{th} arm with respect to the central backbone.

The torsion of each CTR tube can be derived from the third component of the equation that describes the curvature for a single tube [14]:

$$\begin{aligned} u'_{z_{i,j}} = & u_i'^* + \frac{(EI)_{i,j}}{GJ_{i,j}}(u_{x_{i,j}}u^*_{y_{i,j}} - u_{y_{i,j}}u^*_{x_{i,j}}) + \\ & \frac{(G'I)_{i,j}}{(GJ)_{i,j}}(u^*_{z_{i,j}} - u_{z_{i,j}}) - \frac{1}{(GJ)_{i,j}}\mathbf{e}_3\mathbf{R}^T_{i,j}\mathbf{l}. \end{aligned} \tag{8}$$

The resulting curvature of the pull/pull segment $\mathbf{u}(s)$ and position $\mathbf{r}(s)$ are unknown and are estimated as the function of the length tubes of the navigation section. The total arc length of each rod can be estimated as:

$$\ell_k = \int_0^l \|\boldsymbol{r}'_k(s)\| \mathrm{d}s, \tag{9}$$

where $\|.\|$ denotes the ℓ_2-norm and $\mathbf{r}_k(s)$ is the position of k^{th} rod given by

$$\boldsymbol{r}_k(s) = \boldsymbol{r}_{k=1}(s) + \mathbf{R}(s)\boldsymbol{d}_k. \tag{10}$$

Substituting (10) in (9) and simplifying the equations using (3) yields

$$\ell_k = \int_0^l \|\boldsymbol{e}_3 + [\mathbf{u}(s)]_\times \boldsymbol{d}_k\| \mathrm{d}s. \tag{11}$$

The shape of each tubular component belonging to one of the CTR arms is given by:

$$\boldsymbol{r}_{i,j}(s) = \boldsymbol{r}_{k=1}(s) + \mathbf{R}(s)\boldsymbol{p}_j. \tag{12}$$

To get the shape of the CTR arms, the end position and orientation of the central backbone of the navigation is employed to define the initial posture of the CTR arms as well as the torsion of the previous section along with tube's angle, $\theta_{i,j}$. Following the approach of [14], the curvature of the most exerted tube of the j^{th} arm is:

$$\begin{aligned} \mathbf{u}'_1 = & -\mathbf{K}^{-1}\sum_{i=1}^{n} \mathbf{R}_{\theta_i}(\mathbf{K}_i(\theta'_i \frac{\mathrm{d}\mathbf{R}^T_{\theta_i}}{\mathrm{d}\theta_i}\mathbf{u}_1 - \mathbf{u}_i'^*) + [\mathbf{u}_i]_\times \mathbf{K}_i \\ & (\mathbf{u}_i - \mathbf{u}^*_i) - \mathbf{K}^{-1}([\boldsymbol{e}_3]_\times \mathbf{R}_1^T \int_s \mathbf{f}_s(\sigma)\mathrm{d}\sigma + {\mathbf{R}_1}^T\mathbf{l}). \end{aligned} \tag{13}$$

In (13) we dropped the subscript j^{th} for simplicity. The torsion of each tube is described in (8).

Equations (3), (7), (8), (11) and (13) comprise the system of differential equations governing the motion of the robot. The system of equations are solved as a boundary value problem with the following boundary conditions:

$$\boldsymbol{r}(0) = [0\ 0\ 0]^T, \tag{14a}$$
$$\mathbf{R}(0) = \mathbf{I}, \tag{14b}$$
$$\ell_k(0) = 0, \tag{14c}$$
$$\ell_k(l) = L_k,\ k \neq 1, \tag{14d}$$
$$u_{xy_{i,j}}(s = \ell) = u^*_{xy_{i,j}}. \tag{14e}$$

Additional constraints arise from the continuity that should be enforced at the multiple bending segments and at the transition points of the CTR arms. The appropriate conditions across each transition point should be enforced and are defined as:

- the position and orientation of the backbone and each CTR arm must be continuous *i.e.*,

$$\boldsymbol{r}(s^-) = \boldsymbol{r}(s^+), \quad \mathbf{R}(s^-) = \mathbf{R}(s^+), \tag{15}$$

- the torsion of each arm's tubular component should be continuous across its length around z direction:

$$u_{z,ij}(s^-) = u_{z,ij}(s^+), \tag{16}$$

- the balance of moment should be respected:

$$m_{z,ij}(s^-) = m_{z,ij}(s^+). \tag{17}$$

A. Solution Approach

The model is defined by (3), (7), (8), (11) and (13) with the boundary conditions and constraints described in (14), (15), (16) and (17). It accepts the overall length of the rods that comprise the navigation section of the robot L_k as inputs and computes the shape of the central backbone. It also accepts the length of tubes that comprise the CTR arm so to get the shape of the rest of the tubular components. However, while the initial curvature along x and y direction *i.e.* $u_{xy}(0)$ is unknown, the length of the rods of the push/pull segments are known and defined both at the base ($s = 0$) and the end of each segment. In addition, the curvature of the CTR arms at the end of the navigation section is unknown, with the curvature at its distal point known and equal to the precurvature of the most exerted tube.

The model presented in Sec. II is quasi-static and solved using the separation of variables. Such an approach is acceptable in cases where the velocity and acceleration of the system is low and dynamic phenomena are avoided.

The differential equations can be solved using standard methods such as the Runge-Kutta family of algorithms, while the boundary value problem can be solved by non-linear root-finding (shooting) methods.

III. System Design and Prototyping

This section describes the design and engineering of the robotic system prototype. The system was designed for the evaluation of the proposed theoretical work and consists a proof of concept for the ultimate employment of hybrid robotic systems for surgical interventions. The system comprises one bending push/pull segment and up to 3 CTR arms. Figure 3 shows the developed robotic system while important robot's dimensions are shown in Table I.

The navigation part of the end-effector is a 2 DoF segment section that is actuated by two nitinol (NiTi) tubes with outer diameter (OD) of 0.69 mm and inner diameter (ID) of 0.45 mm, which are passed through holes located on fixtures. The fixtures, with a diameter of 9 mm, are employed to guide the manipulation arms and avoid buckling of the tubes. They were 3D-printed by Formlabs Form 3B. A PVC rod shown in beige in Fig. 1 is acting as the central backbone. It has a diameter of 2 mm and is rigidly connected to the fixtures to ensure that they cannot move relative to each other. The length of the navigation section is 83 mm.

TABLE I

Physical parameters of the robot.

$l_{k=1}$	83 mm	E_{NiTi}	80 MPa
l_{11}	46 mm	G_{NiTi}	15 MPa
l_{21}	41 mm	$D_{\text{inner rod}}$	0.33 mm
l_{12}	47 mm	OD/$ID_{i=2,j}$	$0.69/0.45$
l_{22}	35 mm	$D_{\text{k=1}}$	2 mm
u^*_{2j}	23 m^{-1}	OD/$ID_{\text{tube push/pull}}$	$1.2/0.8$
u^*_{1j}	32 m^{-1}	D_{fixtures}	9 mm

The tubes are actuated by continuous RS motors (SRC SM-S4315R) with a maximum torque of $1.47\,\text{Nm}$. The translation of each tube is monitored via the employment of linear, continuous turn, rotary potentiometers. The motors are connected to lead screws which convert the power generated by the motors to linear velocity of the push/pull tubes. The motors are connected to the lead screws via the employment of flexible coupling to absorb also any possible misalignment. The lead screws are carrying 3D printed parts, printed in a WASP 2040 with PLA material, that are connected rigidly to the push/pull tubes.

The manipulation section can accommodate up to 3 concentric tube robot arms. It was chosen to employ 3 CTR arms based on the discussion in [3]. In any intervention, it is preferred to be able to have bimanual manipulation and the ability to visualize the tools and the area of surgical interest. It is envisioned that one arm will be able to hold a camera while the other two a surgical tool. Each arm comprises an outer tube and an inner rod, both made of NiTi. The outermost tube has an outer diameter of 0.67 mm and inner diameter of 0.45 mm while the diameter of the rod is 0.33 mm. Both tubular components are precurved with the outer tube precurved at approximately $23\ \text{m}^{-1}$ and the inner one with a precurvature of around $32\ \text{m}^{-1}$.

Each tubular component is able to be rotated and translated independently. Continuous RS motors (SRC SM-S431R) are employed for the translation of each tube while servo motors (DS3235) with maximum torque of $3.43\,\text{Nm}$ and range from $0^\circ - 270^\circ$ are selected for the rotational DoFs. Stainless steel (SS) tubes are selected for the transmission of the manipulation arms. It is chosen to limit the length of the NiTi by gluing it to a straight and stiffer SS tube, reducing the torsional effect which can result to snapping which is the sudden motion of the tubes from one configuration to another due to accumulation of energy. As the SS tubes are stiffer than the NiTi tubes, the danger of having snapping is minimized. The translational DoF is monitored by continuous turn, linear potentiometers while for the rotational DoF a timing belt is used. Timing belts can retain the compactness of a system however they come with the problem of blacklash. To avoid such an effect, a pretenser is employed to adjust

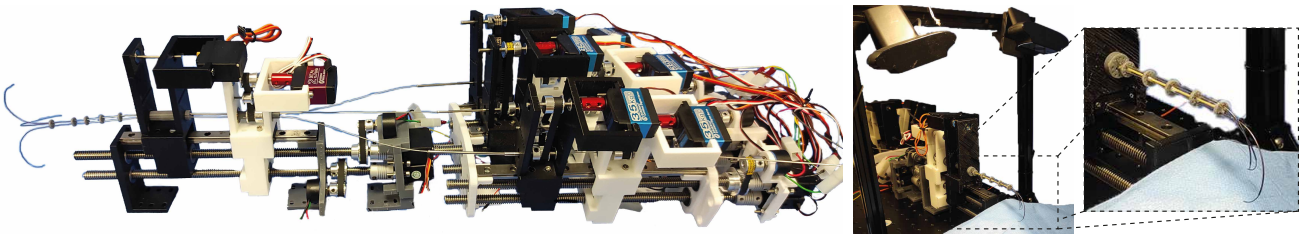

Fig. 3. **Left:** The developed robot prototype. The actuation unit comprises the subsystem for the actuation of the manipulation arms and the subsystem for the actuation of the navigation section. Each CTR arm is actuated by an identical module. **Right:** The stereo vision system used to capture the end-effector's shape to verify the theoretical model.

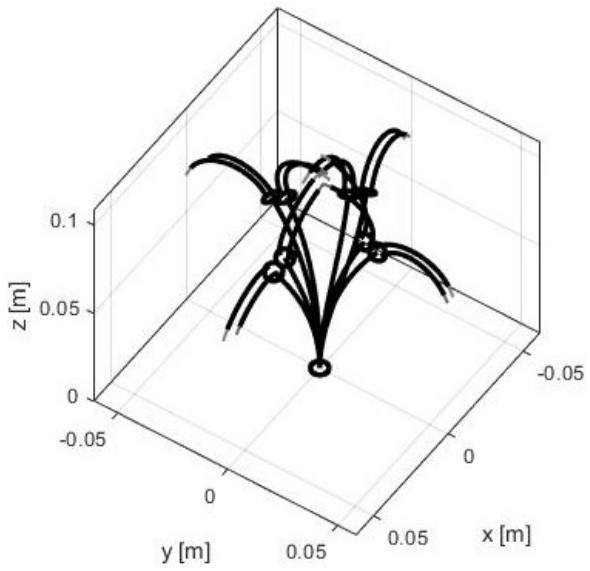

Fig. 4. Workspace of the hybrid robot for actuation input of 1.5 mm and 2 mm in each rod's direction.

the pretension of the timing belt.

IV. Experiments & Theoretical Analysis

A set of experiments was performed with the robotic system prototype to evaluate the model developed in Sec. II. It was preferred to accommodate here two CTR arms for facilitation of data analysis and assembly of the end-effector. We examined the model's fidelity considering various configurations with and without loading conditions.

A. Workspace Analysis

Each rod of the push/pull section was actuated by an arbitrary value to showcase the robot's workspace for that value. Here, we chose to actuate each rod (push and pull) by 1.5 mm and 2 mm respectively and rotate each arm by 180°. Figure 4 showcases the configurations of the hybrid end-effector for those values. Different values of actuation of the push/pull section can eliminate the interior boundary of the workspace and achieve a convex workspace meaning that the CTR arms can reach with enhanced dexterity regions close to vertical axis of the end-effector as well as far away from it as can be seen by Fig. 4.

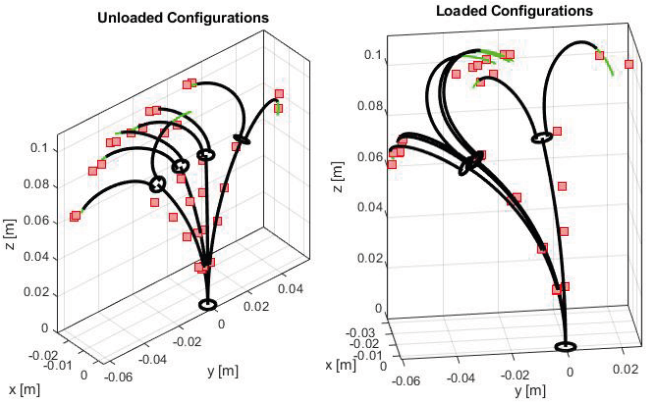

Fig. 5. The shape of the central backbone and two CTR arms derived via simulations for 4 configurations with (left) and without (right) load. The red markers show the actual position of the fixtures and tubes' end for each configuration.

B. Stereo Vision System

The accuracy of the proposed model was evaluated using a stereo pair setup (Logitech HD Pro C922), shown in Fig. 3. The stereo pair was calibrated using MATLAB's calibration toolbox. The mean reprojection error attained for each camera was 0.33 pixels.

To estimate the error of the developed model, sequences of image pairs were captured in which the robot was actuated by a different value. For each image pair, we manually selected 4 distinct corresponding points in the images and performed stereo triangulation using the Direct Linear Transformation [22]. This resulted in a set of initial 3D points, which were then refined by minimising the reprojection error on each image pair. Each of the point that was selected corresponded to the end of each tubular component of the CTR arms. A point corresponding to the most proximal point of the end-effector was selected as reference point to register the reference frame of the stereo vision system to the one in the simulation while the axis were rotated to manage the coordinate frame of the simulations (the z axis is tangent to the central backbone) .

C. Unloaded Experiments

We captured 38 different robot configurations without external load on the robot. For each configuration, the translation of the tube's carriage under actuation was measured and imported as input to the model. The experimental position

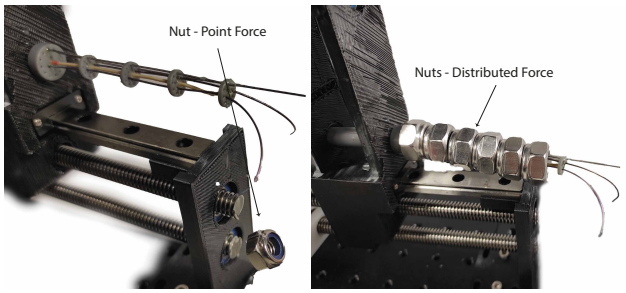

Fig. 6. The experimental setup to simulate external forces. **Left:** Weight in the end of the outer tube of the right arm, **Right:** Distributed weight on the navigation section.

of each one of the CTR arms was measured via the stereo vision system and compared to the simulated one.

Results of the measurements including maximum, mean, standard deviation of error of the model in predicting the robot's shape are listed in Table II. Figure 5 shows that the simulated shape of the central backbone and CTR arms can capture well the actual position of the fixtures and tubes' end. It should be noted that all the errors are normalized with respect to the length of the end-effector.

The mean error per unit length was found to be 3.64%, attaining a maximum of 7.61% and standard deviation of approximately 1.62%. Figure 5 depicts the shape of the central backbone via simulations. There, the red markers show the position of the fixtures as derived by the stereo vision system. It can be observed that the developed model can also predict the shape of the push/pull section. Figure 7 shows the statistical analysis of the errors.

D. Loaded Experiments

To demonstrate the capability of the model to capture the shape of the end-effector under external forces, a set of 32 experiments with a distributed force and a point force on the outer tube of the right arm was performed. The weight of end-effector is negligible and does not lead to noticeable deformation. We employed a number of nuts which were placed along the length of the push/pull segment as can be seen in Fig. 6. The overall weight of the nuts was approximately 87g in the first 5 experiments and 73g in the rest 11 experiments. The motion of the nuts along the backbone during its "bending" was on the order of 1mm, therefore not noticeably affecting force distribution. The points of interest for model evaluation where never covered by nuts. A final set of 16 experiments were run with a point force on the outer tube of the right CTR arm. We employed a nut weighted 4.7g to emulate the point force. Table II shows the error in the loaded experiments. The mean error in the loaded experiments found to be 3.47% per unit length, close to the state of the art models for non-hybrid robots. It is should be noted that the error here is lower than the error in the unloaded experiments due to the different actuation inputs. Figure 5 shows that the model can predict the actual shape of the end-effector under loaded conditions too.

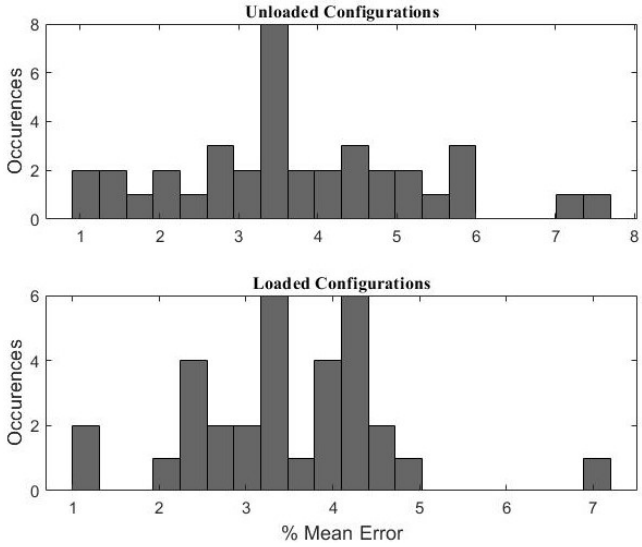

Fig. 7. Histogram of the mean error for the unloaded configurations (above) and for the loaded cases (bottom).

TABLE II

EXPERIMENTAL RESULTS. MAXIMUM ERROR OF TIP POSITION (e_{max}), MEAN ERROR OF TIP POSITION (e_{mean}), STANDARD DEVIATION OF ERROR (σ). ALL THE ERRORS ARE NORMALIZED PER UNIT LENGTH

	$\%e_{max}$	$\%e_{mean}$	σ
Unloaded exp.	7.61	3.64	1.62
Loaded exp.	7	3.47	1.14

V. CONCLUSION

In this work, the design and modelling of a novel continuum robot was presented. It is a hybrid continuum robot combining push/pull and concentric tube technology. This miniaturized single-port system is able to deliver multiple arms through a push/pull actuated segment. The hybrid multi-arm continuum robot promises to make more interventions accessible and less invasive as it combines the stiffness of a push/pull system with the dexterity and the small diameter of CTRs. To prove the concept of a hybrid robot, we designed a system with a 2 DoF push/pull segment and 3 CTR arms with each one of them comprising two NiTi tubes with 4 DoF in total. It is envisioned that this kind of robot can be used in interventions in which a flexible navigation section is required to achieve enhanced dexterity and flexibility [3].

A new model for the hybrid continuum robot was also developed and presented in this manuscript. The model is based on the Cosserad rod theory and can predict the overall shape of the end-effector via an end-to-end quasistatic model. The developed theory can model the robot's end-effector with an overall error (taking into account the loaded and unloaded cases) of 3.56% per unit length as can be seen from the statistical analysis in Fig. 7.

Future work pertains to investigating intricate behaviours of this class of robots, such as elastic stability and relate them to design parameters through the development of bespoke robot design algorithms.

REFERENCES

[1] J. Burgner-Kahrs, D. C. Rucker, and H. Choset, "Continuum Robots for Medical Applications: A Survey," *IEEE Transactions on Robotics*, vol. 31, no. 6, pp. 1261–1280, 2015.

[2] G. Fagogenis, M. Mencattelli, Z. Machaidze, B. Rosa, K. Price, F. Wu, V. Weixler, M. Saeed, J. E. Mayer, and P. E. Dupont, "Autonomous robotic intracardiac catheter navigation using haptic vision," *Science Robotics*, vol. 4, no. 29, 2019.

[3] Z. Mitros, S. Sadati, C. Seneci, E. Bloch, K. Leibrandt, M. Khadem, L. D. Cruz, and C. Bergeles, "Optic Nerve Sheath Fenestration with a Multi-Arm Continuum Robot," *IEEE Robotics and Automation Letters*, vol. 5, no. 3, pp. 4874–4881, 2020.

[4] T. L. Bruns, A. A. Remirez, M. A. Emerson, R. A. Lathrop, A. W. Mahoney, H. B. Gilbert, C. L. Liu, P. T. Russell, R. F. Labadie, K. D. Weaver, and R. J. Webster, "A modular, multi-arm concentric tube robot system with application to transnasal surgery for orbital tumors," *International Journal of Robotics Research*, vol. 40, no. 2-3, pp. 521–533, 2021.

[5] W. Wei, R. E. Goldman, H. F. Fine, S. Chang, and N. Simaan, "Performance evaluation for multi-arm manipulation of hollow suspended organs," *IEEE Transactions on Robotics*, vol. 25, no. 1, pp. 147–157, 2009.

[6] Z. Mitros, B. Thamo, C. Bergeles, L. da Cruz, K. Dhaliwal, and M. Khadem, "Design and Modelling of a Continuum Robot for Distal Lung Sampling in Mechanically Ventilated Patients in Critical Care," *Frontiers in Robotics and AI*, vol. 8, no. May, 2021.

[7] P. J. Swaney, A. W. Mahoney, A. A. Remirez, E. Lamers, B. I. Hartley, R. H. Feins, R. Alterovitz, and R. J. Webster, "Tendons, concentric tubes, and a bevel tip: Three steerable robots in one transoral lung access system," in *Proceedings - IEEE International Conference on Robotics and Automation*, vol. 2015-June, no. June, 2015, pp. 5378–5383.

[8] N. Sarli, G. D. Giudice, S. De, M. S. Dietrich, S. D. Herrell, and N. Simaan, "TURBot: A System for Robot-Assisted Transurethral Bladder Tumor Resection," *IEEE/ASME Transactions on Mechatronics*, vol. 24, no. 4, pp. 1452–1463, 2019.

[9] Z. Mitros, S. Sadati, R. Henry, L. daCruz, and C. Bergeles, "From Theoretical Work to Clinical Translation: Progress in Concen-tric Tube Robots," *Annual Review of Control, Robotics, and Autonomous Systems*, 2021.

[10] I. A. Gravagne and I. D. Walker, "Kinematic transformations for remotely-actuated planar continuum robots," *Proceedings - IEEE International Conference on Robotics and Automation*, vol. 1, no. April, pp. 19–26, 2000.

[11] Y. Chen, B. Wu, J. Jin, and K. Xu, "A Variable Curvature Model for Multi-Backbone Continuum Robots to Account for Inter-Segment Coupling and External Disturbance," *IEEE Robotics and Automation Letters*, vol. 6, no. 2, pp. 1590–1597, 2021.

[12] N. Simaan, K. Xu, W. Wei, A. Kapoor, P. Kazanzides, R. Taylor, and P. Flint, "Design and Integration of a Telerobotic System for Minimally Invasive Surgery of the Throat," *International Journal of Robotics Research*, vol. 28, no. 9, pp. 1134–1153, 2009.

[13] E. Amanov, J. Granna, and J. Burgner-Kahrs, "Toward improving path following motion: Hybrid continuum robot design," in *Proceedings - IEEE International Conference on Robotics and Automation*, 2017, pp. 4666–4672.

[14] D. C. Rucker, B. A. Jones, and R. J. Webster, "A geometrically exact model for externally loaded concentric-tube continuum robots," *IEEE Transactions on Robotics*, vol. 26, no. 5, pp. 769–780, 2010.

[15] P. E. Dupont, S. S. Member, J. Lock, B. Itkowitz, E. Butler, and S. S. Member, "Design and control of concentric-tube robots," *IEEE Transactions on Robotics*, vol. 26, no. 2, pp. 209–225, 2010.

[16] C. Bergeles, A. H. Gosline, N. V. Vasilyev, P. J. Codd, P. J. Del Nido, and P. E. Dupont, "Concentric tube robot design and optimization based on task and anatomical constraints," *IEEE Transactions on Robotics*, vol. 31, no. 1, pp. 67–84, 5 2015.

[17] Z. Mitros, M. Khadem, C. Seneci, S. Ourselin, L. Da Cruz, and C. Bergeles, "Towards modelling multi-arm robots: Eccentric arrangement of concentric tubes," in *2018 7th IEEE International Conference on Biomedical Robotics and Biomechatronics (Biorob)*, 2018, pp. 43–48.

[18] L. Wang, F. C. Pedrosa, and R. V. Patel, "Eccentric-tube robot (etr) modeling and validation," in *2020 8th IEEE RAS/EMBS International Conference for Biomedical Robotics and Biomechatronics (BioRob)*, 2020, pp. 866–871.

[19] J. Wang, J. Peine, and P. E. Dupont, "Eccentric tube robots as multiarmed steerable sheaths," *IEEE Transactions on Robotics*, pp. 1–15, 2021.

[20] S. S. Antman, *Nonlinear Problems of Elasticity Second Edition*, 2005, vol. 107.

[21] A. Bajo and N. Simaan, "Hybrid motion/force control of multi-backbone continuum robots," *The International Journal of Robotics Research*, vol. 35, no. 4, pp. 422–434, 2016.

[22] R. Hartley and A. Zisserman, *Multiple View Geometry in Computer Vision*, 2nd ed. USA: Cambridge University Press, 2003.